

Scalable overset computation between a forest-of-octrees- and an arbitrary distributed parallel mesh

HANNES BRANDT, Rheinische Friedrich-Wilhelms-Universität Bonn, Germany

CARSTEN BURSTEDDE, Rheinische Friedrich-Wilhelms-Universität Bonn, Germany

We introduce an algorithm that performs a one-directional mesh overset of a parallel forest of octrees with another distributed mesh of unrelated partition. The forest mesh consists of several adaptively refined octrees. Individual smooth mappings for every tree allow to represent a broad range of geometric domains. The other mesh is generic and defines a distributed set of query points, e.g. stemming from a quadrature rule applied to each cell. We face the problem of finding data for all queries in the remote forest.

The forest is partitioned according to its natural Morton ordering. Thus, the partition boundaries can be encoded globally with one Morton index per process, which allows for precise, communication-free searching of the queries in the partition geometry. This is necessary to organize non-blocking communication of the queries to the relevant processes only. In a subsequent local search of the forest, we process the incoming queries and return the data of interest to each query's origin.

The algorithm can be generalized, for example to load balancing of the overset, or adaptive refinement of the meshes around their intersection area. In 2D and 3D example scenarios we demonstrate the algorithm's performance and scalability to 12,288 processes.

CCS Concepts: • **Theory of computation** → **Sorting and searching**; **Computational geometry**; • **Mathematics of computing** → **Mathematical software performance**; • **Computing methodologies** → **Massively parallel algorithms**; *Distributed algorithms*; **Distributed simulation**; **Massively parallel and high-performance simulations**; • **Applied computing** → *Physics*.

Additional Key Words and Phrases: Adaptive mesh refinement, forest of octrees, mesh overset, remote search

1 Introduction

Many physical systems are modeled using multiple computational meshes. A common example are Computational Fluid Dynamics (CFD) models around multiple, sometimes deforming, objects, e.g. for simulations of wind farms [Kirby et al. 2019] or rotorcraft [Jarkowski et al. 2014]. A single mesh approach would require complicated geometric operations or frequent re-meshing. Instead, multiple meshes can be used in the Chimera grid method [Steger et al. 1983] (also known as mesh overset).

Next to the aforementioned geometrical considerations, a multi-mesh simulation can also be motivated by physical properties of the system, e.g. when several physics layers interact. For example, this occurs when modeling acoustic and gravity waves stemming from seismic sources [Zettergren and Snively 2019]. The waves originate on earth and pass through the lower atmosphere as well as the ionosphere. An efficient approach is to subdivide the domain into two overlapping parts and to

The authors gratefully acknowledge partial support under DARPA Cooperative Agreement HR00112120003 via a subcontract with Embry-Riddle Aeronautical University. This work is approved for public release; distribution is unlimited. The information in this document does not necessarily reflect the position or the policy of the US Government.

We acknowledge additional funding by the Bonn International Graduate School for Mathematics (BIGS) as a part of the Hausdorff Center for Mathematics (HCM) at the University of Bonn. The HCM is funded by the German Research Foundation (DFG) under Germany's excellence initiative EXC 59 – 241002279 ("Mathematics: Foundations, Models, Applications"). We acknowledge further funding by the DFG under grant no. 467255783 ("Hybride AMR-Simulationen").

We would also like to acknowledge access to the "Bonna" and "Marvin" compute clusters hosted by the University of Bonn. Authors' Contact Information: Hannes Brandt, Rheinische Friedrich-Wilhelms-Universität Bonn, Bonn, Germany, brandt@ins.uni-bonn.de; Carsten Burstedde, Rheinische Friedrich-Wilhelms-Universität Bonn, Bonn, Germany, burstedde@ins.uni-bonn.de.

employ separate solvers for atmosphere [Snively 2013] and ionosphere [Zettergren and Snively 2015]. In particular, this allows the solvers to operate in different coordinate systems to facilitate efficient solutions for each model.

To obtain physically meaningful results, the solvers of a multi-mesh simulation must yield consistent solutions in their overlap regions. Thus, they generally exchange simulation results, most commonly by first searching and then interpolating solution data from one mesh to the other.

In the context of the Chimera grid method this process is referred to as donor search [Noack et al. 2009; Roget and Sitaraman 2014]. This procedure is commonly accompanied by a hole profiling step, where cells lying inside the solid body described by another mesh are identified. Additionally, cells are assigned donor and receptor roles by choosing the cell with the most accurate solution.

In this paper we consider mesh overset for applications like the geophysical simulation described above. There, hole profiling is not required as the domains do not define holes. Furthermore, it is sufficient to pass interpolated data only from the ionosphere model to the lower atmosphere model, resulting in an inherently one-directional process without any need for cell-based role assignment. Consequently, in the scenario considered the overset consists of a donor search combined with interpolation and communication of the results.

There is a variety of donor search algorithms for different mesh types. For uniform, structured grids the donor cell can be computed directly. For unstructured grids of various element types, more intricate solutions are required. Known strategies start with structuring the search space by storing it in a coarse grid [Hedayat et al. 2022; Roget and Sitaraman 2014], a K-d tree [Horne and Mahesh 2019], an Alternating Digital Tree [Noack et al. 2009; Roget and Sitaraman 2014; Schluter et al. 2005; Suhs et al. 2002] or an octree [Gagnon 2022]. After narrowing down the search space using such structures, a line walk [Noack et al. 2009; Roget and Sitaraman 2014], a stencil jump [Suhs et al. 2002] or an exhaustive search [Roget and Sitaraman 2014] can be applied to identify the actual donor.

Many mesh overset approaches employ distributed-memory parallelism to allow for simulations on large scale clusters. This introduces another obstacle to the donor search as now donor cells have to be identified across processes. Some approaches address this issue by replicating the query points on all processes [Schwarz 2005] or by identifying target processes for the query points based on axis-aligned bounding boxes of the mesh partitions [Horne and Mahesh 2019]. Other approaches distribute the domain such that overlapping meshes end up on the same process [Roget and Sitaraman 2014; Shibliyev and Sezai 2021; Zhao et al. 2024].

This paper is concerned with the mesh overset of octree-based meshes. Octrees are already commonly used in overset methods as structured, axis-aligned (often called background) meshes [Jude et al. 2021; Péron and Benoit 2013], to organize and load balance domain decomposition methods [Shibliyev and Sezai 2021], for hole profiling [Noack and Kadanthot 2002] or as a structure for process-local donor searches [Gagnon 2022]. However, their parallel search capabilities in combination with the geometrical flexibility of a mapped forest-of-octrees structure have not yet been explored fully in the overset context.

We consider a forest-of-octrees structure [Burstedde et al. 2011], which only stores the leaves of the trees, thus avoiding the memory overhead of maintaining several overlapping levels of cells and associated data. For parallel distribution, a linear ordering of all leaf cells according to the Morton space-filling curve [Morton 1966] is split into consecutive sub-ranges of equal size, resulting in a partitioning fit for large scale parallel applications. By applying smooth mappings to the trees, a forest can represent a broad range of geometric domains [Burstedde et al. 2013]. Hence, forests of octrees can serve not only as background mesh, but also as adaptive, curvilinear 'near-body' meshes.

In the following chapters, we will introduce an efficient, scalable algorithm performing mesh overset of a parallel distributed forest of octrees with an unstructured mesh of unrelated partition, which consists of elements of arbitrary type. The unstructured mesh is represented by parallel distributed sets of points, e.g. stemming from a quadrature rule applied to each cell, for which evaluation data is queried from the forest.

The Morton-order based partitioning scheme allows for efficient donor searches in the parallel distributed forest of octrees. The exact partition boundaries of the mesh can be deduced from the first local tree and Morton indices on every process. We utilize this to efficiently search the queries in the forest partition [Burstedde 2020] and thereby assign each point to its donating process. Subsequently the points are searched in the local part of the forests employing a top-down tree traversal for multiple query points at once [Isaac et al. 2015]. By applying the inverse mapping of a tree to all query points – similar to [Henshaw and Schwendeman 2008; Noack et al. 2009] – we are able to avoid expensive intersection tests with curved cells.

The back-and-forth messaging of the query points between the unstructured mesh communicator and the forest communicator is based on non-blocking, point-to-point communication. Thus, computation and communication are overlapped and load imbalances are partially compensated. Additionally, the linear Morton ordering of the leaf cells allows for precise and flexible repartitioning of the forest. By assigning weights to each cell according to its overset workload and performing a weighted repartitioning, the load balance of the overset can be improved significantly. The overset can be performed for congruent but also for disjoint or partially overlapping mesh communicators.

The algorithm is defined in a modular manner by treating query points as black box, user-defined structures, that are handled by user-defined intersection tests and evaluation functions. Thus, it can be repurposed with ease, e.g. for the weight computation of the load balancing procedure or for adaptive refinement of both meshes around their intersection area.

To summarize, we introduce an efficient, scalable, parallel distributed one-directional mesh overset algorithm for forests of octrees with an unstructured second mesh. Tree-wise smooth mappings allow the forest mesh to cover curvilinear, adaptive domains, as required for a near-body mesh. The Morton-order based partitioning of the forest cells can be leveraged for scalable donor searches in the distributed mesh and allows for easy yet effective load balancing of the overset. The proposed algorithm was implemented in the forest of octrees library p4est [Burstedde 2010] and tested for various artificial test cases, showcasing near optimal scalability up to 12,288 cores. It is applicable as is to simulations requiring a one-directional exchange, e.g. in acoustic and gravity wave modeling.

2 A Distributed Forest Data Structure

The focus of this paper is on mesh overset scenarios that include at least one distributed forest of octrees. In this chapter we will give a minimal overview of a representer data structure and its key properties that our overset algorithm relies on. For a comprehensive set of notation and definitions we refer to [Isaac et al. 2015].

First, we will present a general notion of forests of octrees and describe how the Morton order can be used to maintain a total order and distribute the octrees' cells [Burstedde et al. 2011]. Then we will review search operations on octrees, both in a process local [Isaac et al. 2015] as well as in a global manner [Burstedde 2020]. The ability to search parallel distributed points in a parallel distributed forest of unrelated partition is a key element to our proposed algorithm.

2.1 Distributed Forests of Octrees

We define each octree on the cubic reference domain $[0, 2^b]^3$. Here, an octree is a tree with root $[0, 2^b]^3$ and maximum level b in which each interior node has exactly eight children, which are

derived by splitting the parent node in half in every dimension. The nodes of the tree are called *octants*. The two-dimensional counterpart of an octree is a *quadtree*, which divides each interior *quadrant* into four children. All algorithms presented in this paper work with both octrees and quadtrees.

A *forest of octrees* can be seen as the conforming decomposition of a geometric domain in physical space into $K \in \mathbb{N}$ subvolumes. Each subvolume indexed by $k \in \mathbb{N}$ with $0 \leq k < K$ is an octree mapped from the reference domain into physical space by a diffeomorphism $\psi_k: [0, 2^b]^3 \rightarrow \mathbb{R}^3$. The possibility to combine large amounts of trees with individual smooth mappings allows to represent a broad range of geometric domains, of which a sphere or a torus (quadtrees mapped to a 2D surface in 3D) are relatively trivial examples.

In a linear forest of octrees [Sundar et al. 2008] only the leaf octants, which form a partition of the domain, are associated with data (e.g. physical quantities). The interior nodes are regarded as virtual objects that cover a cubical subtree of cells. They are not stored at all, but rather created on the fly whenever needed. Under this paradigm, distributing a forest of octrees comes down to distributing its leaves.

The key to efficient partitioning of a forest of octrees is a total order of the leaf octants induced by a space-filling curve. We use a recursive level-wise lexicographical order known as the Morton order [Morton 1966]. By combining the Morton index m of the front lower left corner coordinates of an octant with its level ℓ and tree index k we obtain a total order over (k, m, ℓ) . Thereby, the task of distributing a forest of octrees to a set of P processes can be reduced to the task of partitioning the linear ordering of all leaf octants into contiguous subranges. This simplifies and accelerates load balancing tremendously.

To describe the global partition, every process $0 \leq p < P$ shares k_p and m_p of its local octant with lowest global index as the tuple (k_p, m_p, ℓ_p) . The volume of the tree belonging to process p is uniquely defined by (k_p, m_p, b) and (k_{p+1}, m_{p+1}, b) , where we use the maximum-resolution level b for simplicity. By gathering the set

$$\mathbf{F} := \{(k_p, m_p, b) \mid p = 0, \dots, P-1\} \cup \{(K, 0, b)\} \quad (1)$$

of *global first positions* on every process, we can exactly determine how the reference and the geometric domain are distributed between the processes without any further communication [Burstedde 2020; Burstedde et al. 2011]. This is a key capability for remote searching in distributed forest of octrees. An example of a partition and how it is encoded by the global first positions is displayed in Figure 1.

2.2 Searching in Distributed Octrees

The mesh overset algorithm requires efficient searching of parallel distributed sets of points in the distributed forest of octrees. Here, the distribution of the points may not match the distribution of the forest at all. A communication-free *partition search* [Burstedde 2020] can assign each local point to the process it intersects and thereby help organizing communication. After all points are sent away and received by their respective processes, they can be searched process-local and assigned to a leaf octant [Isaac et al. 2015].

2.2.1 Process-local Search. Each process p owns a contiguous subrange of the global ordering of the leaf octants with range $[\mathbf{F}_p, \mathbf{F}_{p+1}) = [(k_p, m_p, b), (k_{p+1}, m_{p+1}, b))$. To search in the local part of the forest the trees in the range $[k_p, k_{p+1}]$ are traversed in a top-down manner for multiple points simultaneously, starting at the root with the complete set of local query points. At each recursion the current octant gets tested against all points that passed at its parent. Only the points that yield a potential match get passed on to its children.

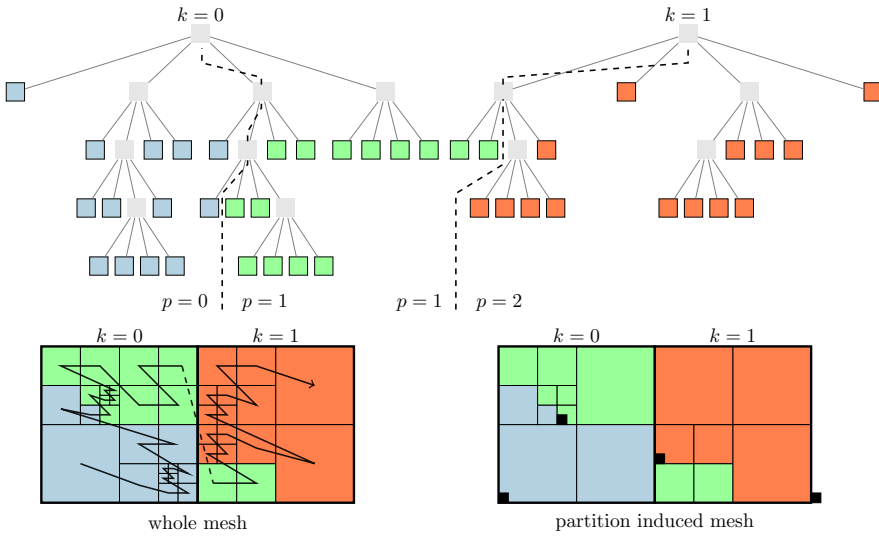


Fig. 1. Example of a forest of $K = 2$ quadrees (top) and the corresponding mesh in the geometric domain (bottom left). The black arrow shows the ordering of the mesh quadrants according to the Morton space-filling curve. In this example the curves of both trees have the same orientation, but this is not necessarily so. The mesh is partitioned among three processes represented by colors and divided by black dashes. The mesh on the bottom right is the coarsest mesh suited to represent the partition boundaries exactly. It can be deduced communication-free from the global first positions (small, black cells) and is the basis of the partition search, even without ever being constructed explicitly.

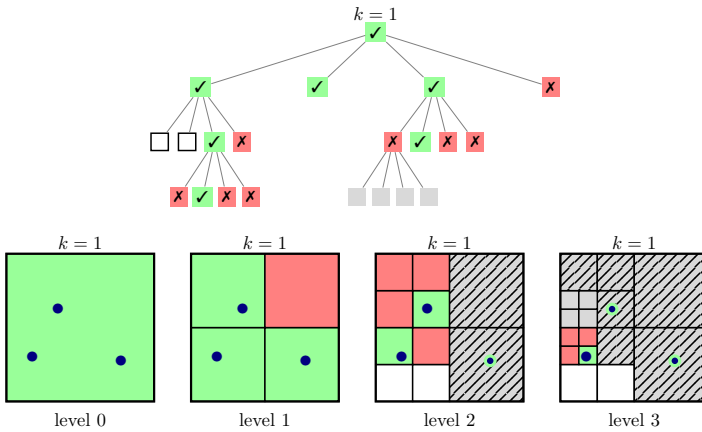


Fig. 2. Local search of three points (blue) on process 2 in the example forest from Figure 1, shown for the tree k_1 (top) and the corresponding part of the mesh (bottom). Green cells containing a check mark indicate at least one point in the given quadrant. Red cells containing a cross indicate no match. A gray cell indicates that the quadrant was not part of the search, either because it was visited before (hatched cells) or an ancestor cell yielded no match (plain cells). Cells in the tree belonging to a different process are white. The four meshes on the bottom describe the execution of the search by increasing levels of the tree.

The root and all other interior octants are constructed temporarily on the fly. Simultaneously, the contiguous subsection of the linear leaf array that intersects the current interior octant is tracked and updated [Isaac et al. 2015]. For octants that do not intersect the range $[F_p, F_{p+1})$ at all the recursion stops immediately. An example of this *local search* can be seen in Figure 2.

The search algorithm can be defined in a rather general manner by treating points as anonymous structures and relying on a user-defined callback function

$$\text{Local_Match}(\text{query point } \text{qpoint}, \text{octant } o, \text{flag } \text{isLeaf}). \quad (2)$$

to decide which points intersect which octant. The function has to return `true`, if `qpoint` may match with a descendant of `o` or `o` itself, and `false`, if this is certain to not be the case. For interior nodes of the tree, where `isLeaf` is `false`, the callback may rely on fast, possibly false positive tests. On the leaves, the callback is expected to check for exact matches.

This general approach allows for searching for a variety of objects, ranging from points to rays, polygons, to any shape at all, legally intersecting multiple cells at the same time.

2.2.2 Partition Search. The local search described in the previous section is sufficient to search a globally available set of points in a distributed forest of octrees. However, if the points are distributed, e.g. because there are too many to store them on a single process or they originate from a distributed structure, a partition search is required. This search routine operates on the global first positions F and assigns points (or any object rather) to the process(es) they are contained in. The fundamental difference to the local search is that it has no access to, and thus does not reference, any leaves at all.

Similar to the local version the partition search traverses trees in a top-down manner searching multiple points simultaneously. The difference lies in the parts of the forest that are traversed. The partition search operates on all trees and stops the recursion as soon as an interior or leaf octant belongs to a single process p , so it is contained in the range $[F_p, F_{p+1})$. Instead of a leaf octant with associated data it assigns just a process number to each point. An example of the partition search can be seen in Figure 3.

Similar to the local search the algorithm relies on a callback

$$\text{Partition_Match}(\text{query point } \text{qpoint}, \text{octant } o, \text{rank } \text{pfirst}, \text{rank } \text{plast}). \quad (3)$$

The parameters `pfirst` and `plast` that get passed to the `Match` callback describe the range of processes contributing to the current interior octant. The search stops for `pfirst = plast`. Thus, `pfirst` and `plast` have a similar role to the `isLeaf` flag in `Local_Match`. They are continuously updated during the forest traversal, splitting F into increasingly smaller index ranges.

Since the global first positions F are available globally and they uniquely determine the partition boundaries, the partition search, like the local search, operates communication-free.

3 Overset Algorithm

In this section we proceed to detail all parts of the proposed parallel mesh overset algorithm. Its general flow is depicted in Figure 4, and its key steps are specified in the following sections.

First, we will describe the problem setup of the mesh overset, which assumes representing general meshes by parallel distributed sets of *query points*. Then we will characterize how the partition and the local search from Section 2 can be used for searching distributed query point sets in the forest-of-octrees mesh, before taking a closer look at the communication between the two meshes.

3.1 Problem Setup

The proposed algorithm executes the overset of two meshes with at least one of them, namely the mesh that is queried, being a distributed forest of octrees. It performs a one-directional mesh

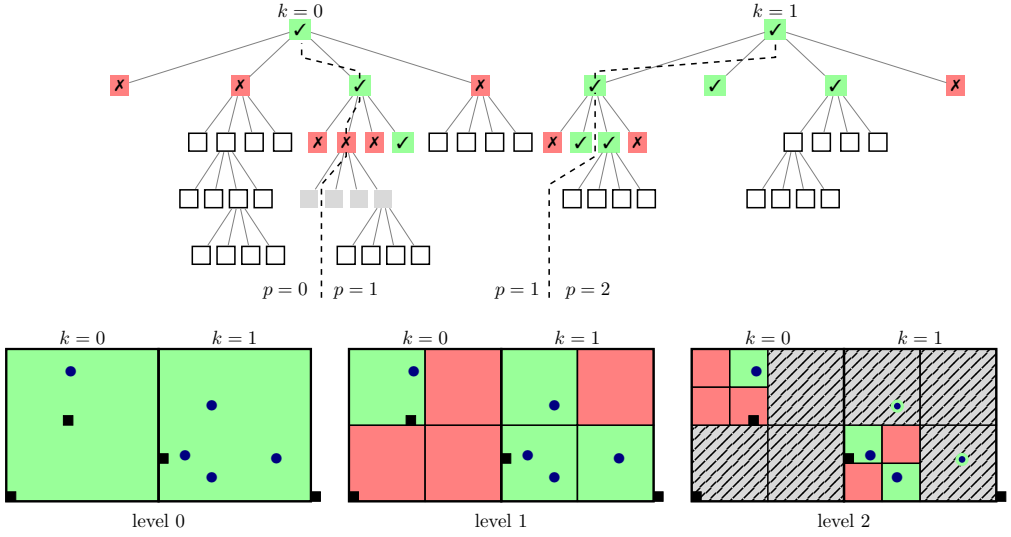


Fig. 3. Partition search of five points (blue) in the example forest from Figure 1, shown for both the trees (top) and the corresponding part of the mesh (bottom). Green cells containing a check mark indicate at least one point match in the given quadrant. Red cells containing a cross indicate no match. A gray cell indicates that the quadrant was not part of the search, either because it was visited before (hatched cells) or an ancestor cell yielded no match (plain cells). The global first positions (small, black cells) mark partition boundaries and thus trigger refinement of the search tree. Cells whose parent belongs to exactly one process cannot occur in the partition search and are marked in white. The search can be imagined to operate on the partition-induced tree from Figure 1. The three meshes on the bottom describe the behavior of the search on the different levels of the tree. Level 3 was omitted since the search does not touch it.

overset, where the roles of the two meshes are unambiguously distinguished, and may serve as a building block for alternating or synchronous two-directional mesh overset algorithms.

A set of query points Q originating from a generic mesh is to be located in a separate forest-of-octrees mesh to retrieve data. How the query points are derived from the generic mesh is entirely up to the user. A common case would be to instantiate a quadrature rule in every one of its cells. Strictly speaking, we would not even require any notion of mesh in the first place but might think directly of a distributed parallel point cloud. According to its role, we refer to this possibly unstructured mesh (or point cloud) as the *consumer*.

We assume that each octant of the forest of octrees is associated with data of interest, for example computed using a user-defined solver. Our goal is to provide this data to the consumer by evaluation at its query points, for example through interpolation of the solver’s results. Therefore, we refer to the forest of octrees as the *producer*. We do not make any assumptions on the nature of the interpolation – our algorithm is generic over any kind of information.

Both meshes may reside on congruent or on distinct sets of processors with different numbers of processes. We denote the process count of the forest of octrees by P and the process count of the consumer mesh by Q . Consequently, we call a producer process p and a consumer process q . A parallel distributed consumer mesh leads to parallel distributed sets of query points Q_q that form a partition of Q . So, the set of query points Q_q passed into the algorithm is a different one for every process q .

Whether and where the producer and consumer mesh intersect depends on how they are mapped into physical space. As described in Section 2.1, the forest of octrees is transformed from the

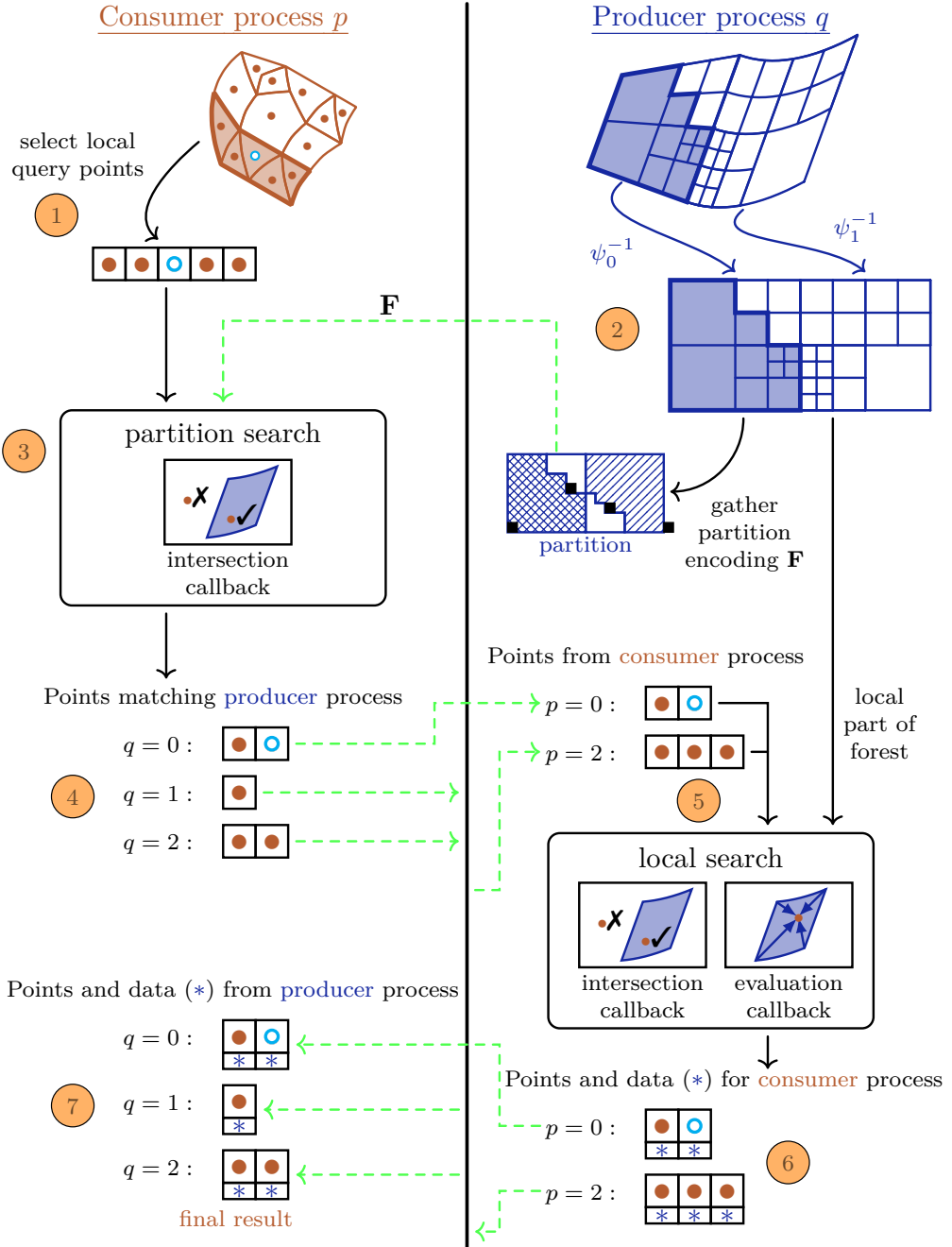


Fig. 4. Flowchart of the mesh overset algorithm. The chart shows the local computations of rank 0 of both the consumer (left, orange) and producer (right, blue) communicator as well as the communication they participate in (green, dashed lines). One query point is highlighted as a light blue circle during the whole algorithm. The numbers in orange circles offer a proposed reading order of the flow chart. The various steps are exposed in detail throughout Section 3.

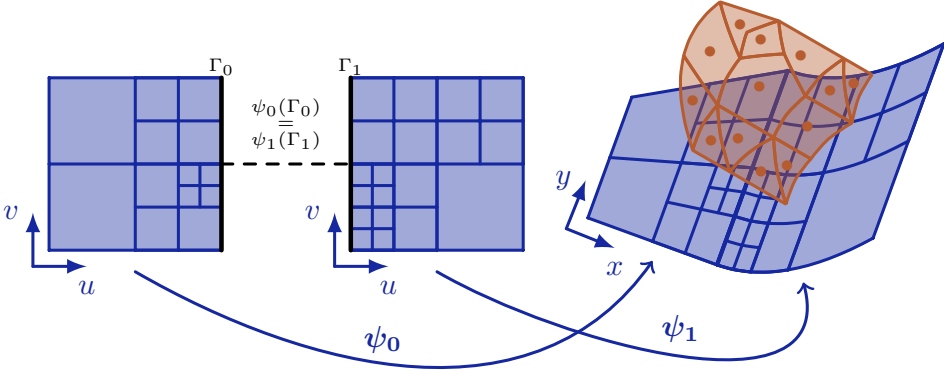


Fig. 5. Example for the geometric setup of the mesh overset. The consumer side is displayed in orange and the producer side in blue. The consumer mesh is unstructured and consists of triangles, quadrilaterals and a pentagon. We have one query point for every cell center. The producer mesh is a forest of two octrees. Both (square) reference domains are mapped to physical space by a mapping ψ_k , respectively. The resulting geometric domain is connected, since the trees intersect precisely at the edge $\psi_0(\Gamma_1) = \psi_1(\Gamma_2)$. Note that the parallel partition and distributed nature of the two respective meshes is *not* shown in this display.

reference space into physical space by smooth functions ψ_k , with k being the index of the tree. This is just a convention, however, and we leave the definition of geometry entirely to the application.

How the consumer mesh is mapped into physical space only affects the creation of the query points. Namely, before passing the points to our algorithm, they have to be converted into the same physical coordinate system that the forest of octrees maps to. In practice, this means that some knowledge of the producer's geometry definition must be made available, hardcoded or communicated, to the consumer. Only when the producer's geometry metadata is distributed in parallel, we may incur the need to define an intermediate reference coordinate system, which we do not detail here for simplicity. An example setup for the mesh overset is displayed in Figure 5.

We may summarize the objective as to provide every consumer process q with the evaluation result for all of q 's query points \mathbf{Q}_q that intersect any producer's domain in physical space. To this end, we will specify two black-box operations that the user must define and implement, (a) an intersection query of a point with a hypothetical octant and (b) an evaluation query that returns the data for a query point when it is found to be in a specific octant of the producer mesh.

3.2 Partition Search of Query Points

After the specification of the query points, each consumer process q owns a process-local set \mathbf{Q}_q with coordinates in the producer physical space. However, the solution data required for evaluation resides on the producer side. Accordingly, the query points need to be sent to the correct producer process.

Naively, this might be achieved by gathering the query points from all consumer processes on all producer processes. For congruent mesh communicators, such would be achieved by an Allgather call. For disjoint mesh communicators, each consumer process might send its points to every producer process via the global communicator resulting in a communication scheme similar to an Alltoall between the communicators.

However, these schemes would result in predominantly unnecessary communication, since each query point obtains its evaluation data from at most one producer octant and thereby at most

one process. Furthermore, they would exhaust the available memory already on moderately sized parallel simulations. Thus, we proceed in a decidedly tighter fashion.

3.2.1 Proposed Approach. Our method proceeds in two stages centered around a remote and a local mesh search. With the information available on the consumer side we cannot determine the exact octant, because we do not know the producer forest’s leaf structure. Nonetheless, we can assign the point to the process that contains the octant by use of the partition search described in Section 2.2.2. This only requires knowledge of the global first positions \mathbf{F} of the producer forest, which are cheaply communicated, as well as the forest connectivity and geometric mappings, which can be compiled into the consumer or otherwise shared. We exemplarily describe the interchange for disjoint communicators in Section 3.4 and its implementation in Appendix A.

Algorithm 1: Partition_Match (query point \mathbf{qpoint} , octant o , rank \mathbf{pfirst} , rank \mathbf{plast})

```

1: if Intersection_Test( $o$ ,  $\mathbf{qpoint}$ , ( $\mathbf{pfirst} = \mathbf{plast}$ )) then
2:   | if  $\mathbf{pfirst} = \mathbf{plast}$  then
3:     |   |  $\mathbf{Q}_{q,p} \leftarrow \mathbf{Q}_{q,p} \cup \{\mathbf{qpoint}\}$       /* add  $\mathbf{qpoint}$  to send buffer for process  $p$  */
4:     |   | return true
5:   | else
6:     | return false

```

The partition search allows us to split the set \mathbf{Q}_q into P disjoint sets $\mathbf{Q}_{q,p} \subseteq \mathbf{Q}_q$ containing the query points from consumer process q that require information from producer process p . To accomplish this, we provide a callback function Partition_Match (Algorithm 1) satisfying the call convention defined in Section 2.2.2. Since we are searching for the donor of the query point \mathbf{qpoint} , we only return true if the octant o may contain \mathbf{qpoint} , which we delegate to a user-defined callback

$$\text{Intersection_Test}(\text{octant } o, \text{query point } \mathbf{qpoint}, \text{boolean exact}). \quad (4)$$

The intersection test must be provided by the application and may be over-inclusive if $\mathbf{pfirst} \neq \mathbf{plast}$ (exact is false), but it has to yield the precise result when there is only one participating process left for the given \mathbf{qpoint} . The reason is that we wish to send \mathbf{qpoint} only to the one process it lies in, thus eliminating false positives.

During the partition search every process creates and constantly updates the P sets $\mathbf{Q}_{q,p}$ local to process q , which all start out empty. Since we request an accurate intersection test when $\mathbf{pfirst} = \mathbf{plast}$, every point will appear in at most one set if we apply a proper tie breaking rule around octant boundaries. The points that lie outside of the producer domain will not appear at all.

When the partition search is complete, $\mathbf{Q}_{q,p}$ contains all query points that have to be sent to producer process p for evaluation.

3.2.2 Intersection Test. The callback in Algorithm 1 depends on the mappings ψ_k applied to the forest of octrees as well as the representation of the query points.

As mentioned in Section 3.1, the query point \mathbf{qpoint} is given in the producer physical coordinate system. Thus, it is a straightforward approach to transform the octant o into the same system by use of the mapping ψ_k of the producer tree containing o . However, in some cases this can result in curved edges and faces of the mapped octant which complicates the intersection test and might even require solving a system of nonlinear equations.

To avoid this, in many cases we can inversely map \mathbf{qpoint} into the reference space of o instead, which is a common approach for donor searches in curvilinear grids [Henshaw and Schwendeman

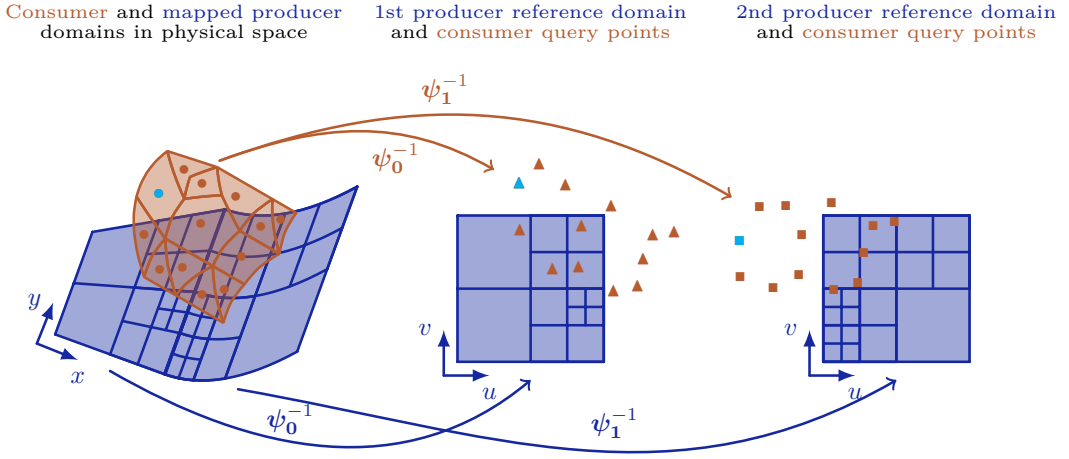


Fig. 6. Example for the query point search in the reference domain. This continues the problem setup introduced in Figure 5. The consumer side is displayed in orange and the producer side in blue. The query points originate in the consumer mesh. They are mapped to the reference domain by applying ψ_k^{-1} for every producer tree k . The points for tree 1 are represented by \blacktriangle and the points for tree 2 by \blacksquare . The resulting point clouds differ due to the different inverse mappings. Should the inverse map of points outside the reference image be undefined, we would expect the user to detect and discard these points ahead of time.

2008; Meakin 1991; Noack et al. 2009]. This technique can be applied to mapped forests of octrees as well. The key advantage of this approach is that it allows for easy and accurate intersection tests since all octant faces are planar and axis-aligned in the reference domain. Especially, it comes with negligible additional cost to perform accurate tests at every level. Due to the efficiency of the axis-aligned tests, computing ψ_k^{-1} of qpoint may be the most time consuming part of the Intersection_Test. However, it has to be computed and stored only once each time the search enters a new tree k . An example of this approach is displayed in Figure 6.

While the inverse mapping approach can be beneficial in many cases, it has to be handled with care. For example, ψ_k^{-1} may not be defined for query points outside of the mapped producer domain. In this case, a tree intersection test in the producer physical coordinate system preceding the actual tree recursion can help to ensure that we only inversely map points inside the image of ψ_k . If no explicit formula for ψ_k^{-1} is available, a Newton iteration may be employed to approximate ψ_k^{-1} for any point.

3.2.3 Technical Intricacies. When implementing the intersection test, potential floating-point errors need to be considered and handled. This is the case even for the axis-aligned test based on inverse mappings: Octant boundaries are in $([0, 2^b] \cap \mathbb{Z})^3$ and can be represented exactly either as an integer or as a double. However, the application-dependent inverse mapping of the query point may still be subject to floating-point errors. This may result in a query point lying on an octant boundary inside the mesh not being found by any of the adjacent octants.

To avoid missing any point inside the mesh, we recommend a tolerance to the intersection test. Thus, neighboring octants ‘overlap’ around their shared faces, edges or corners. This approach causes new inaccuracies in the search procedure, as a query point may now be found in several octants. However, this can be dealt with by removing the point from the search once it was found in any octant. Under the assumption of the evaluation function being smooth, erroneously assigning a point to a direct neighbor octant causes only a moderate error.

If the tolerance leads us to identify a direct neighbor process by a small margin, we must make sure that the ensuing process-local search, described below, is guaranteed to match within that tolerance to not lose the point.

3.3 Local Search and Evaluation

After the partition search, the query points are sent from their respective consumer processes to the producer process that contains the data for them. How to determine the communication pattern will be elaborated upon further in Section 3.4. For now, we assume that a given producer process p has received $Q_{q,p}$ from consumer process q .

Due to the intersection tests on the leaves of the partition search tree being accurate, all incoming points are contained in the local part of the producer forest of octrees. We can apply the local search routine described in Section 2.2.1 to all received points simultaneously.

Algorithm 2: Local_Match (query point $qpoint$, octant o , flag $isLeaf$)

```

1: if Intersection.Test( $o, qpoint, isLeaf$ ) then
2:   | if  $isLeaf$  then
3:     |    $qpoint \leftarrow Evaluate\_Solution(o, qpoint)$       /* result stored in  $qpoint$  */
4:     |   return true
5: else
6:   | return false

```

Similar to the partition search, we define a Local_Match callback function according to the convention of the search routines described in 2.2. It accepts the $isLeaf$ flag in lieu of the $pfirst$ and $plast$ arguments. The function may reuse the inverse intersection test from Section 3.2. Again, the test may yield over-inclusive results except when on the leaves of the search tree, which is indicated by the $isLeaf$ flag.

If a query point intersects a leaf octant, we can start with the actual evaluation of the solution data for the point, which is performed by a user-defined callback function

$$Evaluate_Solution(octant\ o, query\ point\ qpoint). \quad (5)$$

Since the leaf octant is part of the local forest, we can assume that the solution data is available on this process, which was generally not the case during the partition search. Finally, we store the resulting evaluation data in the query point structure it belongs to. Afterwards, we send the resulting, data-augmented query point buffer $Q_{q,p}^*$ back to consumer process q .

3.3.1 Technical Intricacies. Similar to the partition search, floating-point errors need to be considered when it comes to implementing the intersection test in the local search. Again, adding a tolerance to the axis-aligned intersection test is a sensible approach.

The subdivision of the global search routine into partition and local search introduces another potential error source to the system. Based on the results of the partition search the consumer process q should receive evaluation data from producer process p for every query point in $Q_{q,p}$. It is desirable to preserve this property despite potential floating-point errors.

Thus, we have to make sure every query point found in the partition search is found in the local search, too. To achieve this, we relax the tolerance in the local search by a factor of two in relation to the partition search.

The partition search compares the query points to the shallower octants including roots, while the local search compares them to the deeper octants including leaves. Thus, the tolerances may not be chosen relative to the octant's size. Instead, the tolerance should be a constant below the minimum octant size, e.g. $t = 1000\epsilon$ for the partition and $2t$ for the local search with machine ϵ .

3.4 Communication

During the mesh overset all query point buffers $\mathbf{Q}_{q,p}$ are sent from consumer process q to producer process p . Eventually, the resulting updated buffers $\mathbf{Q}_{q,p}^*$ have to be returned. Since we allow overlapping or even congruent producer and consumer communicators, a process might assume both roles at the same time. Therefore, we need to intertwine consumer and producer communication steps in a way that avoids any potential deadlocks and race conditions.

The pseudocode of the resulting algorithm is displayed in Algorithm 3. There, unlike in the rest of this paper, p denotes not a producer, but a global rank which may be a consumer, a producer or both. We use background colors to distinguish between the different roles p may assume. The orange lines are only executed when p is a consumer rank, the blue lines are only executed when p is a producer rank, and the neutral lines are executed when p is both. The inputs \mathbf{Q}_p and f_p are considered to be \emptyset or NULL, respectively, if p does not have the corresponding role.

3.4.1 Partition Search and Notification. If the consumer and producer mesh reside on congruent communicators, the partition search operates communication-free [Burstedde 2020]. For disjoint communicators we cannot avoid communication completely, because we need to send the $P + 1$ global first positions \mathbf{F} , which encode the partition of the forest of octrees, from the producer to the consumer side. To achieve this, rank 0 of the producer communicator sends \mathbf{F} to rank 0 of the consumer communicator. Then the consumer rank 0 broadcasts the information to all processes in its communicator. This scheme may be optimized further, but there is usually no need.

Algorithm 3: Overset (local query point array \mathbf{Q}_p , dist. forest of octrees f_p , callback `Intersection_Test`, callback `Evaluate_Solution`)

```

1:  $\mathbf{Q}_p^* \leftarrow \emptyset, S_p \leftarrow \emptyset$  /*  $p$  represents the current rank,  $q$  any other rank, see Section 3.4 */
2:  $\mathbf{F} \leftarrow \text{Get\_global\_first\_positions}(f_p)$  /* using MPI_Gather and MPI_Broadcast */
3: /* search  $\mathbf{Q}_p$  in  $\mathbf{F}$ , pass callback to Partition_Match (see Algorithm 1) */
4:  $(S_p, (\mathbf{Q}_{p,q})_{q \in S_p}) \leftarrow \text{Search\_partition}(\mathbf{Q}_p, \mathbf{F}, \text{Intersection\_Test})$ 
5:  $\mathcal{R}_p \leftarrow \text{Notify\_receivers}(S_p, (\mathbf{Q}_{p,q})_{q \in S_p})$ 
6: for each  $q \in \mathcal{R}_p \setminus \{p\}$  do
7:   MPI_Irecv ( $q, p, \mathbf{Q}_{q,p}, \text{tag}$ )
8: for each  $q \in S_p \setminus \{p\}$  do
9:   MPI_Isend ( $p, q, \mathbf{Q}_{p,q}, \text{tag}$ )
10: for each  $q \in S_p \setminus \{p\}$  do
11:   MPI_Irecv ( $q, p, \mathbf{Q}_{p,q}^*, \text{tag}^*$ )
12: while  $\exists q: q \in \mathcal{R}_p \setminus \{p\}$  and message  $\mathbf{Q}_{q,p}$  from  $q$  is pending do
13:    $\mathbf{Q}_{q,p} \leftarrow \text{Next\_incoming\_message}(\mathcal{R}_p, \text{tag})$  /* using MPI_Waitsome */
14:   /* search  $\mathbf{Q}_{q,p}$  in  $f_p$ , pass callbacks to Local_Match (see Algorithm 2) */
15:    $\mathbf{Q}_{q,p}^* \leftarrow \text{Search\_local}(\mathbf{Q}_{q,p}, f_p, \text{Intersection\_Test}, \text{Evaluate\_Solution})$  /* local evaluation */
16:   MPI_Isend ( $p, q, \mathbf{Q}_{q,p}^*, \text{tag}^*$ ) /* send back evaluated points */
17: if  $p \in S_p$  then
18:    $\mathbf{Q}_{p,p}^* \leftarrow \text{Search\_local}(\mathbf{Q}_{p,p}, f_p, \text{Intersection\_Test}, \text{Evaluate\_Solution})$  /* special case  $p = q$  */
19:    $\mathbf{Q}_p^* \leftarrow \mathbf{Q}_p^* \cup \mathbf{Q}_{p,p}^*$  /* add updated local query points */
20: while  $\exists q: q \in S_p \setminus \{p\}$  and message  $\mathbf{Q}_{p,q}^*$  from  $q$  is pending do
21:    $\mathbf{Q}_{p,q}^* \leftarrow \text{Next\_incoming\_message}(S_p, \text{tag}^*)$  /* using MPI_Waitsome */
22:    $\mathbf{Q}_p^* \leftarrow \mathbf{Q}_p^* \cup \mathbf{Q}_{p,q}^*$  /* add updated query points */
23: MPI_Waitall ( $S_p \setminus \{p\}, \text{tag}$ ) /* wait for query Isends to complete */
24: MPI_Waitall ( $\mathcal{R}_p \setminus \{p\}, \text{tag}^*$ ) /* wait for reply Isends to complete */
25: return  $\mathbf{Q}_p^*$ 

```

Depending on the application, the mappings ψ_k relevant for the intersection test may also change with time. In this case, the two communicators additionally need to update according to these changes in the same rhythm.

After the partition search, consumer process q has built P sets $\mathbf{Q}_{q,p}$. Some of them might be empty, in which case no message needs to be sent at all. We define

$$\mathcal{S}_q := \{p \in [0, P) \cap \mathbb{Z} \mid \mathbf{Q}_{q,p} \neq \emptyset\} \quad \text{for } q = 0, \dots, Q - 1, \quad (6a)$$

$$\mathcal{R}_p := \{q \in [0, Q) \cap \mathbb{Z} \mid \mathbf{Q}_{q,p} \neq \emptyset\} \quad \text{for } p = 0, \dots, P - 1. \quad (6b)$$

The set \mathcal{S}_q contains all processes consumer process q sends messages to while \mathcal{R}_p contains all processes producer process p receives messages from. However, after the partition search \mathcal{R}_p is not yet known to producer process p . Before the actual exchange of query points can begin, the producer processes need to be notified about their future communication partners \mathcal{R}_p and the corresponding incoming message sizes $|\mathbf{Q}_{q,p}|$. To achieve this, we employ a tree-based communication scheme [Burstedde 2020; Isaac et al. 2012].

3.4.2 Communication of Query Point Sets. After the notification step the actual communication of the query points begins. The communication system may be sparse and irregular: Especially for locality-preserving partitioning schemes – like the Morton order based partitioning employed for the forest of octrees – the process-local part of the mesh covers only a small area of the domain. If similar properties hold for the other mesh’s partitioning, this small area only intersects cells owned by a limited amount of processes. Thus, $|\mathcal{S}_q| \ll P$ and $|\mathcal{R}_p| \ll Q$ is a likely scenario. Consequently, we avoid collective communication whenever possible. Instead, we focus on non-blocking, point-to-point communication using `MPI_Isend` and `MPI_Irecv`.

First, every producer process p posts a non-blocking receive for all messages $\mathbf{Q}_{q,p}$ with $q \in \mathcal{R}_p$. Next, every consumer processes q starts non-blocking sends of these messages. Since process q knows it will eventually receive the updated query point buffers in return, it posts `MPI_Irecv` calls for all $\mathbf{Q}_{q,p}^*$ with $p \in \mathcal{S}_q$ right after.

On the producer side, the actual evaluation process starts now. The producer processes wait for incoming messages using `MPI_WaitSome`. Whenever a message $\mathbf{Q}_{q,p}$ arrives, the process p directly starts a local search of the point set in the local mesh, as it is described in 3.3. We start a separate call to the local search for every $\mathbf{Q}_{q,p}$. Thereby, we miss out on some synergy effects, as we need to traverse the search tree $|\mathcal{R}_p|$ times instead of once, albeit with proportionally less data. However, this minimizes the idle time of producer processes, as they can work on every incoming message immediately. As soon as the local search of $\mathbf{Q}_{q,p}$ is complete, the producer process returns the updated set $\mathbf{Q}_{q,p}^*$ to the consumer process it originated from using `MPI_Isend`.

The consumer processes wait for the arrival of the $\mathbf{Q}_{q,p}^*$, similar to the producer processes, using `MPI_WaitSome`. Whenever messages arrive, they are incorporated into the local query point set \mathbf{Q}_q^* immediately. A quadrature calculation can be executed on the cells for which all evaluation data has already arrived. Finally, all consumer and producer processes wait for their non-blocking sends to complete by a call to `MPI_WaitAll`.

If the consumer and producer communicator overlap, one process may need to send points to itself. Instead, the process can directly access the consumer query point set $\mathbf{Q}_{q,q}$ for its producer local search. Thereby, the evaluation of $\mathbf{Q}_{q,q}$ can be achieved without any communication and executed any time after the sets creation in the partition search and before the end of our algorithm. We place it directly after the local search of all incoming messages sent from consumer processes. Thus, we do not stall the sets $\mathbf{Q}_{q,p}^*$ from being returned to their consumer side origin. At the same time, we cover potential load imbalances of the previous steps, which can lead to consumer processes idling while waiting for the incoming updated query points.

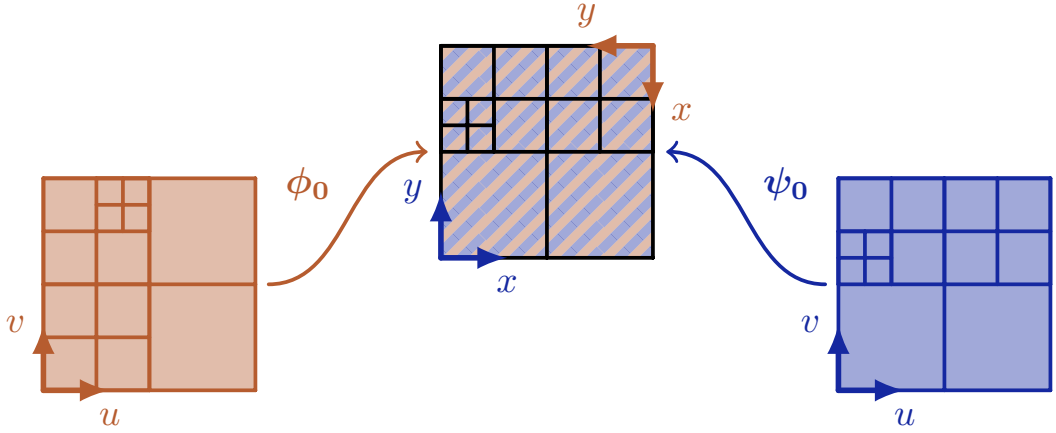


Fig. 7. Geometric setup of the unit square example. The consumer side is displayed in orange and the producer side in blue. Both octrees are mapped to the same domain and refinement pattern in physical space, as indicated by the central, striped mesh and its two $(u, v) \mapsto (x, y)$ coordinate systems.

4 Numerical Applications

In order to test the scalability of the algorithm introduced in the previous Section, we apply it to several artificial examples. We start with a two-dimensional example of two perfectly overlapping meshes based on simplistic mappings. To showcase the algorithm’s capability to deal with highly adaptive meshes, we refine both of them from level 3 to 20. Next, we increase the problems’ complexity by switching to a three-dimensional mapped setting. Here, as an example of a derived novel functionality, we employ the overset algorithm not only for interpolation, but also for guiding the adaptive refinement of the meshes around their intersection area.

Our implementation is realized using the p4est [Burstedde et al. 2011] software library for parallel adaptive mesh refinement on forests of octrees. p4est supplies the octree functionality necessary for our overset algorithm: parallel partition along the Morton curve [Burstedde et al. 2011], mapping of the trees [Burstedde et al. 2011], and partition search [Burstedde 2020] as well as local search routines [Isaac et al. 2015]. All examples are partition independent, which is a key property to ensure reproducibility of the same problem across varying parallel environments. The implementation can be found in the `example/multi` directory of the p4est repository [Burstedde et al. 2010] under the commit b34b7162.

We perform strong and weak scaling tests on the on the Marvin MPP cluster for up to 12,288 processes distributed over 128 compute nodes. Each node contains two 48-core Intel Xeon “Sapphire Rapids” CPUs (2.10 GHz) and 1024 GB of memory. To handle problem inherent load imbalances we introduce a weighted repartitioning, which significantly improves the algorithm’s scalability.

4.1 Unit Square Example

As a first example we consider the 2D mesh overset of two forest-of-quadtree meshes. Both of them are refined adaptively from level 3 to level 20. The consumer forest is designed solely for generating parallel distributed sets of query points.

4.1.1 Simulation Setup. Both the consumer and the producer mesh consist of a single quadtree mapped to the unit square. However, they are mapped in different orientations, as depicted in Figure 7. Thereby, we make sure that even for congruent communicators the local consumer mesh

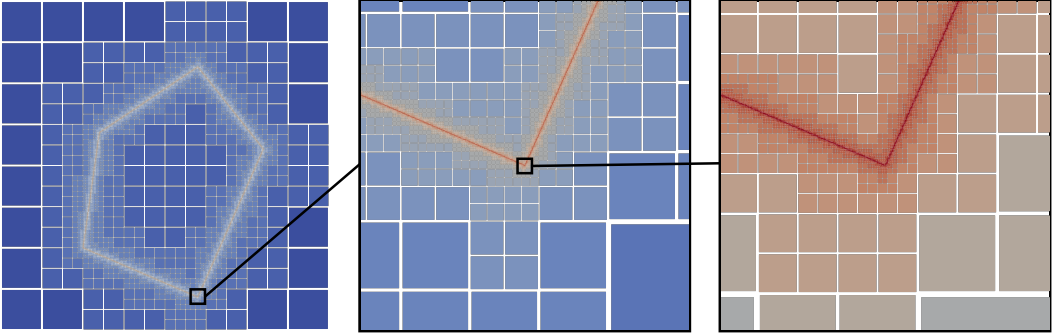


Fig. 8. Levels of the adaptive unit square example. From left to right, the images subsequently zoom to a corner of the pentagon around which the mesh was refined, as indicated by the black boxes. The colors represent the different levels ranging from 3 (blue) to 20 (red).

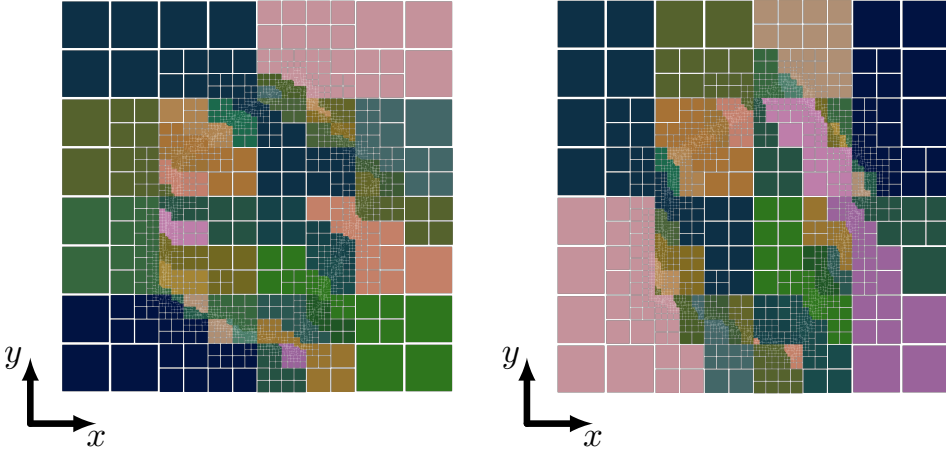


Fig. 9. Partitioning of the producer (left) and consumer (right) mesh for congruent communicators of size $P = Q = 32$ in the adaptive unit square example. The colors encode the partitioning among the processes.

and producer mesh do not overlap perfectly and thus communication is a part of our mesh overset tests. The partitioning of the two meshes is displayed in Figure 9. Starting with the quadtree being refined uniformly to level 2, we iteratively refine all quadrants that intersect the boundary of a given pentagon as long as their level is below 20. Additionally, we ensure a 2:1 balance condition, by refining adjacent quadrants when necessary; see Figure 8.

4.1.2 Numerical Results. We execute the algorithm for 11,432,548 total quadrants per mesh. We conducted scaling tests on the Marvin MPP cluster for up to 3,072 processes distributed over 32 compute nodes.

In order to verify the correctness of the algorithm and its implementation, we compute the approximation error on the cells. Since the adaptive refinement is based on the intersection with a pentagon in physical space both meshes yield the exact same mesh there. Furthermore, we evaluate an artificial function on the cell centers to generate ‘solution’ data on the producer side and also use cell centers as queries on the consumer side. Therefore, we expect the evaluation data we obtain

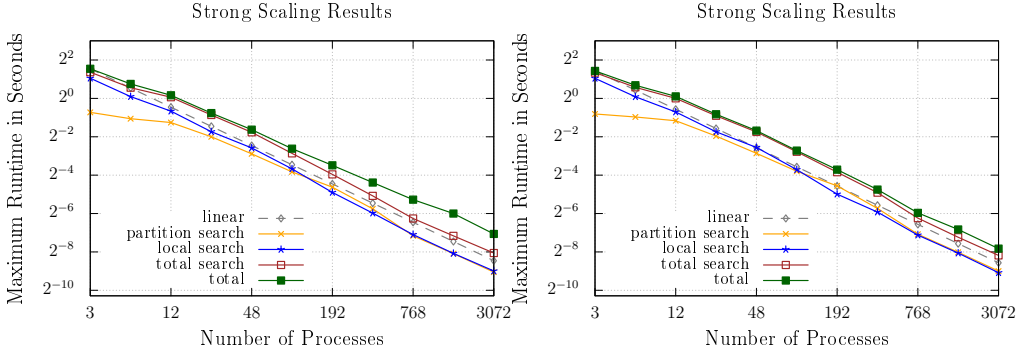


Fig. 10. Strong scaling results of the mesh overset for the adaptive unit square example (left) and its un-rotated alternative (right) on up to 3,072 processes. The mesh overset is performed on congruent mesh communicators. All values represent the maximum time over all processes. We display the total run time including waits (green, filled squares), the time spent in the partition (orange crosses) and local (blue stars) searches (combined: brown squares), as well as linear scaling (gray pluses) for reference.

for a query point to exactly match the solution function when evaluated on its coordinates. The approximation error in the resulting vector’s Euclidean norm indeed remains below 10^{-12} in all test runs.

The results of the strong scaling test are displayed in Figure 10. While for low process counts the increasing complexity of the partition boundaries still has a significant impact on its scalability, the asymptotic behavior is almost linear. The local search scales linearly or even slightly better, due to the recursion depth decreasing with increasing P . The combined complexity of both searches scales almost optimally as well. For low process counts the local search dominates. With increasing P the partition search gains relevance.

The overset is subject to a visible communication overhead. This becomes clear when comparing the test results with the ‘un-rotated’ alternative from Figure 10 (right), where all local queries intersect the local producer forest. Nonetheless, the overall performance of the mesh overset algorithm on this rather extreme mesh pattern appears reliable.

Since the artificial solution is piecewise constant and the evaluation scheme relies on a single evaluation point, the time spent on the evaluation part of the mesh overset is minimized. Its complexity is proportional to the amount of query points received on the producer side. Thus, a more complex evaluation scheme most likely would only improve the observed scalability.

4.2 Arc Example

As a second example we consider the 3D mesh overset of two forests of octrees. Their domains overlap only partially. While the consumer mesh is shaped like a brick, the producer mesh is shaped like an arc. The non-linear mapping of the arc is used to display the viability of the inverse mapping intersection as described in Section 3.2.2. Furthermore, we will use this example setup to demonstrate how the overset from Algorithm 3 can be used for load balancing of the mesh overset as well as adaptive refinement at the boundaries of the intersection area.

4.2.1 Simulation Setup. The consumer mesh consists of 6 octrees connected in a $3 \times 2 \times 1$ ‘brick’, with a mapping that scales, rotates and shifts it. The producer mesh consists of 5 octrees connected in a $5 \times 1 \times 1$ brick format, which is mapped to form an arc.

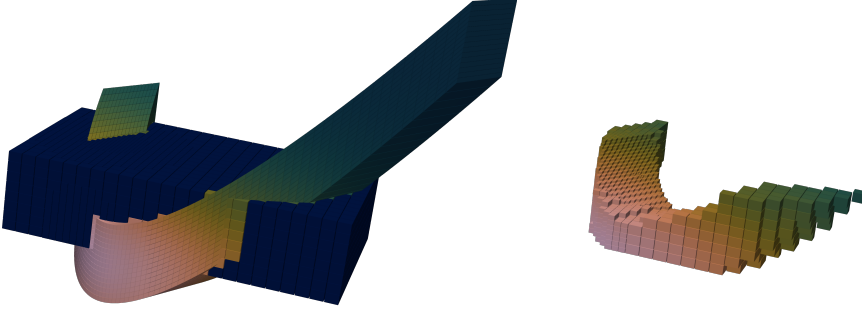


Fig. 11. The color-coded evaluation results of the arc example with artificial evaluation data. The meshes were refined uniformly to level 3 (consumer) and 4 (producer), before being refined adaptively to level 6. We display the consumer and producer mesh overlapping each other (left) and the consumer cells that received evaluation data from the producer (right). It can be seen that a higher resolution of the consumer mesh results in a better approximation of the shape of the arc. Equi-distant color scheme taken from [Cramer2023].

We employ an intersection test, which whenever a query point enters a new tree during the search, applies the tree’s inverse mapping and stores the result in the query point structure. Thus, it is available for all following intersection tests in the same tree. For evaluation of the query points we again use an artificial, piecewise constant solution.

We refine the consumer mesh uniformly to level 7 and the producer mesh uniformly to level 6 before following up with several iterations of adaptive refinement into the region of overlap. As a refinement rule, we compute each octant’s distance to an arbitrary fixed point, which lies inside the intersection area of the meshes, and increase the level for smaller distances, up to a maximum level of 11. This results in several concentric spherical shells of different levels and meshes that are 2:1-balanced by construction. The consumer mesh consists of 2,391,981,241 and the producer mesh of 730,063,983 octants. In a second, smaller test run we start with uniform levels of 5 and 4 and refine to a maximum level of 9, resulting in 37,374,497 consumer and 11,408,346 producer cells. An example of the setup can be seen in Figure 11.

4.2.2 Numerical Results. Similar to the previous examples, we perform a strong scaling test with up to 12,288 processes on 128 nodes of the Marvin MPP cluster.

Again, we start by verifying the correctness of the algorithm and its implementation. Unlike for the unit square example we can no longer assume that we will end up with exact matches between the interpolated overset results and the exact solution data. Instead, we compute a relative error by dividing the norm of the vector of solutions at every query point through the norm of the vector of errors, which meets our expectations as depicted in Table 1.

The results of the strong scaling test are displayed in Figure 12. Similar to the 2D unit square example from Section 4.1.2 the partition search does not scale well going from 3 to 12 processes, but recovers for higher process counts.

The local search however does not scale well anywhere going from 3 to 12,228 processes. This can be explained with the increasing load imbalance in this first version of our problem setup. As can be seen in Figure 11, large parts of both the consumer and the producer mesh are not part of their common intersection area. Processes only owning octants outside the overlap region will not contribute to the mesh overset at all. This effect can also be measured by looking at the maximum number of query points any producer process receives during the overset and how it scales (see Figure 14). While for three processes we have a maximum of 9,609,023 query points with a standard

maxlevel m	7	8	9	10	11
relative ℓ_∞ error	0.1251	0.0612	0.0321	0.0168	0.0086
ratio $m - 1$ to m	-	2.044	1.907	1.911	1.953
relative ℓ_2 error	0.00720	0.00341	0.00168	0.00083	0.00041
ratio $m - 1$ to m	-	2.111	2.030	2.024	2.024

Table 1. Relative error of the mesh overset based interpolation in the ℓ_∞ and the ℓ_2 norm for different maximum level m . The decrease of the error from one level to another is shown as well.

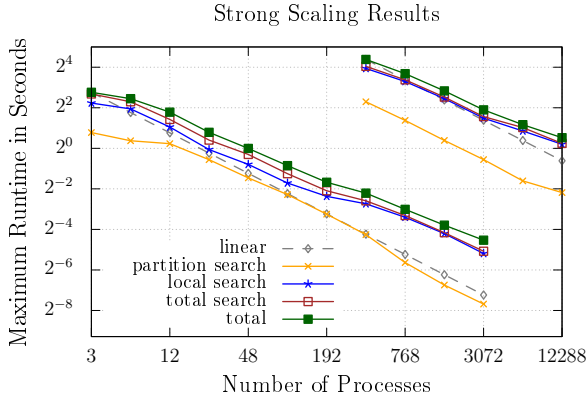


Fig. 12. Strong scaling results of the mesh overset for the arc example without load balancing on up to 12,288 processes. The mesh overset is performed on congruent mesh communicators. We display the maximum run time of the complete mesh overset and some of its substeps. The graphs show total run time (green, filled squares), the time spent in the partition (orange crosses) and local (blue stars) searches (combined: brown squares), as well as linear scaling (gray pluses).

deviation of 10.1%, for 3,072 processes we have a maximum of 115,512 queries with a standard deviation of 103%. So, the maximum number of points to be searched on a single process reduces only by a factor of 83, while the number of processes increases by a factor of 1,024. Thus, the scalability of the mesh overset is limited by the problem’s inherent load imbalances. Luckily, we can tackle load imbalances by a weighted repartitioning approach, as described in the next section.

4.3 Load Balancing

The arc example as described in Section 4.2.1 is subject to significant, problem-inherent load imbalance. Large parts of both the consumer and the producer mesh do not contribute to the intersection area at all, while others contain a mass of high-level octants.

Commonly, parallel mesh overset methods mitigate load imbalance by changing the distribution of grid sub-blocks, e.g. based on bin-packing [Henshaw and Schwendeman 2008] or splitting of the grid sub-blocks into smaller parts [Roget and Sitaraman 2014]. This cannot be done in our mesh overset setup, since the space-filling curve partitioning of the forest of octrees is native to the entire logic. Shifting the partition boundaries in the linear order of octants is the only option, yet a powerful one: To work towards optimal load balance, we perform a weighted repartitioning [Burstedde et al. 2011] of both the consumer and the producer forest of octrees by assigning a weight to every leaf octant representing its workload.

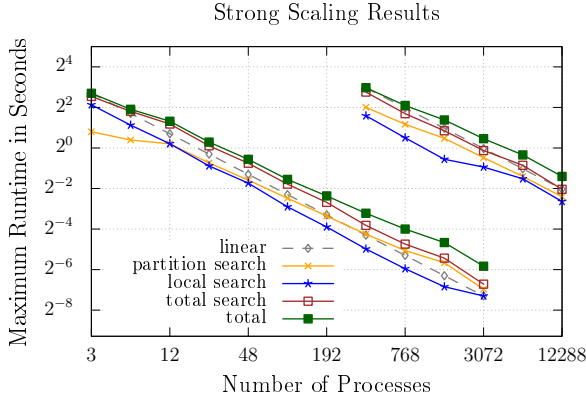


Fig. 13. Strong scaling results of the load-balanced mesh overset for the arc example on up to 12,288 processes. The mesh overset is performed on congruent mesh communicators. We display the maximum run time of the complete mesh overset and some of its substeps. The graphs show total run time (green, filled squares), the time spent in the partition (orange crosses) and local (blue stars) searches (combined: brown squares), as well as linear scaling (gray pluses). The overall run time exhibits significantly improved scalability compared to the unbalanced results from Figure 12. For example, the total run time for 12,288 processes dropped from 1,44s to 0,38s.

We detail our approach as follows. The workload associated with the searches depends strongly on the amount of octant-point intersection callbacks they have to perform. The partition search is executed on the consumer side of the overset algorithm. The partition boundaries and thereby the amount of octants to traverse during the search is the same on all processes and cannot be reduced conveniently. However, the amount of query points entering the search depends on the local consumer octants and is a target well-suited for load balancing.

During the partition search query points that do not intersect the producer domain are part of one intersection test for each of the 5 producer tree roots, before being rejected. Query points that intersect the producer domain are searched until they can be assigned to a unique process, resulting in 8 (or 4 in 2D) intersection tests per search level. To account for this, we add 1 to a leaf octant’s weight for every query point outside the producer domain and a heuristically chosen weight of 7 for each query point inside the producer domain.

The local search is executed on the producer side of the overset algorithm. The amount of points entering the search depends on the local producer octants. Every query point contained in a given producer local leaf octant has to pass through all previous levels of the local forest, resulting in 8 (or 4 in 2D) intersection tests per search level. We add a heuristically chosen weight of 20 for every query point contained in an octant to its base weight of 1.

To compute the consumer and producer octant weights, we strive to determine which query points intersect the producer domain and how many query points intersect any given producer octant. This can be achieved by applying the overset algorithm. We use the same `Intersection_Test` as for a normal mesh overset routine. For evaluation, we use a new callback `Evaluate_Load_Balancing`, which marks the query point to be inside the intersection area and increments the number of queries found in the producer cell.

To test the effect of our heuristic load balancing, we apply it to the test case from Section 4.2.2 and compare the results. The strong scaling of the load balanced run can be seen in Figure 13. The scalability of the mesh overset improves visibly, which also comes with a drop in total run times. For example, the time to compute the overset for $P = 384$ in the larger problem setup reduces from

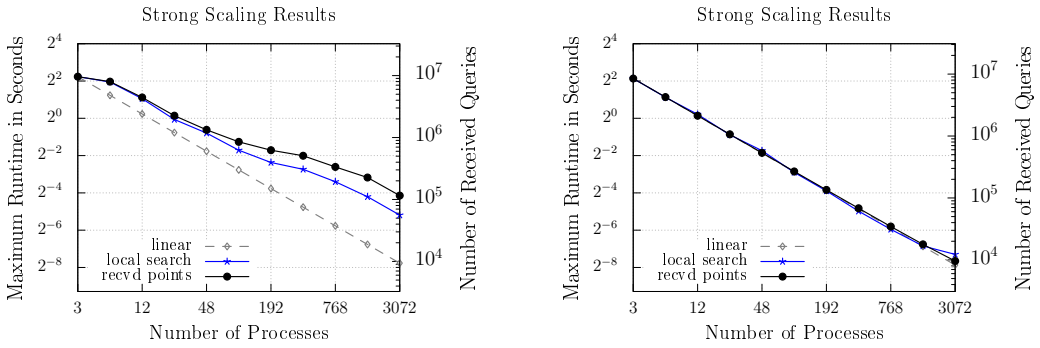


Fig. 14. Comparison of the local search run times of the mesh overset in the non load-balanced (left) and the load-balanced (right) arc example on up to 3,072 processes. The mesh overset is performed on congruent mesh communicators. We display the maximum run time of the local search (blue stars) as well as the maximum number of query points received on any producer process (black circles) and theoretical linear scaling (gray pluses). The significantly improved scalability of the local search underlines the need for load balancing.

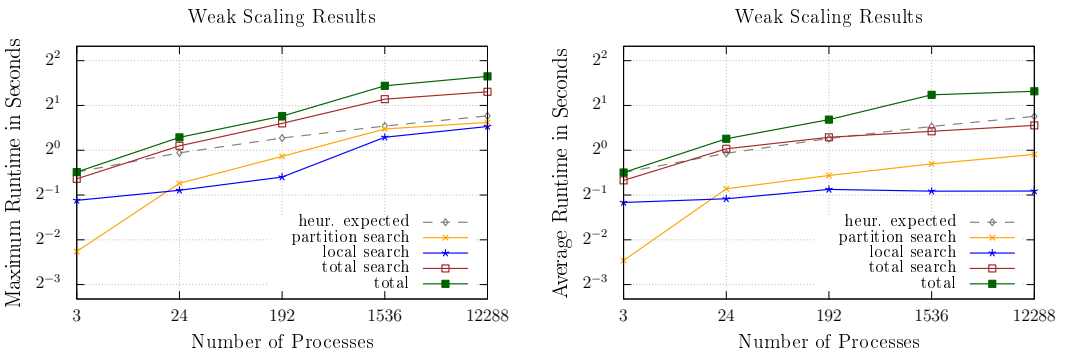


Fig. 15. Weak scaling results of the load-balanced mesh overset for the arc example on up to 12,288 processes. The mesh overset is performed on congruent mesh communicators. We display the maximum run time of the complete mesh overset and some of its substeps in (left) and the average run time in (right). The graphs show total run time (green, filled squares), the time spent in the partition (orange crosses) and local (blue stars) searches (combined: brown squares), as well as heuristically expected scaling (gray pluses).

20.9s to 7.9s. In particular, the local search—which was the main reason for the far-from-optimal results in the unbalanced overset—now scales almost linearly. As can be seen in Figure 14, our repartitioning approach yields the desired results and leads to linear scalability of the maximum amount of queries received on any process.

The improved scalability of the load-balanced overset justifies performing a weak scaling test. Whenever we increase the amount of processes by a factor of eight, we increase the initial uniform level as well as the maximum refinement level by one. The results can be seen in Figure 15. For comparison, the graph contains a heuristic approximation of the workload of searching the the consumer cells in the producer forest.

The weak scalability of the partition search remains the least predictable, which is to be expected, as the partition boundaries get more complex with every step. The local search scales linearly on average.

4.4 Adaptive Refinement Around the Intersection Area

Proper transmission of the solution from one mesh to the other requires sufficient resolution of the receiving mesh – in particular in the intersection area or on its boundary [Kirby et al. 2019]. This can be ensured by adaptively refining the mesh around the intersection area. The overset algorithm presented in this paper can also be used for such refinement, which we demonstrate by refining both the producer and the consumer forest of octrees on the boundary of the intersection area.

We start with marking all boundary octants of the meshes using a flag `o.isBoundary`. Our approach is to set a refinement flag `o.refine` for all producer and consumer leaf octants `o`. We want to set it to **true** if and only if

- `o` intersects an octant from the other mesh and
- at least one of the two octants is a boundary octant in its mesh.

We can not check this criterion precisely without implementing an intersection test for a pair of mapped octants from both meshes, which might cause high theoretical and/or computational effort. Instead, we choose a heuristic approach: We define a set of query points for every consumer cell according to a $3 \times 3 \times 3$ -tensor product. We query the octant’s corners, and the centers of all its faces, edges and volume. Every query point `qpoint` is supplied with its coordinates and the flag `qpoint.isBoundary` inherited from `o.isBoundary`.

Algorithm 4: Evaluate_Refinement (octant `o`, query point `qpoint`)

```

1: if qpoint.isBoundary or o.isBoundary then
2:   | o.refine ← true
3: if o.isBoundary then
4:   | qpoint.wasFound ← 2      /* mark point was found on producer boundary */
5: else
6:   | qpoint.wasFound ← 1      /* mark point was found in producer mesh */
```

This setup allows us to use Overset for the refinement by choosing suitable callbacks. We use the same `Intersection_Test` callback as for a normal mesh overset routine. For evaluation, we use a new callback `Evaluate_Refinement` (see Algorithm 4), which marks both the query point and the octant according to our criterion. After the overset is completed, we check the updated query points for every consumer octant and mark the octant for refinement accordingly. The whole procedure can be seen in Algorithm 5. For simplicity, we consider only congruent communicators, where both the producer forest f_p and the consumer forest g_p are available locally.

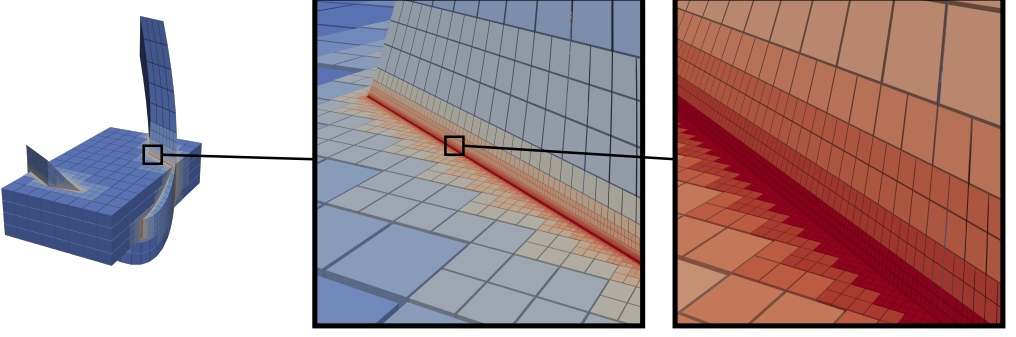


Fig. 16. Color-coded levels of the adaptively refined arc example. From left to right, the images subsequently zoom in onto a part of the boundary of the intersection area, as indicated by the black boxes. The colors represent the different levels going from 2 (blue) to 12 (red).

Algorithm 5: `Set_Refinement_Flags` (producer forest of octrees f_p , consumer forest of octrees g_p)

```

1: Mark_Boundary_Octants( $f_p$ ) /* as described above */
2: Mark_Boundary_Octants( $g_p$ )
3:  $Q_p \leftarrow \emptyset$ 
4: for each octant  $o$  in  $g_p$  do
5:    $Q_p \leftarrow Q_p \cup \text{Query\_Tensor}(o)$  /* query  $3 \times 3 \times 3$ -tensor */
6: for each query point  $qpoint$  in  $Q_p$  do
7:    $qpoint.wasFound \leftarrow 0$ 
8: for each octant  $o$  in  $f_p$  do
9:    $o.refine \leftarrow false$ 
10:  $Q_p^* \leftarrow \text{Overset}(Q_p, f_p, \text{Intersection\_Test}, \text{Evaluate\_Refinement})$ 
11: for each octant  $o$  in  $g_p$  do
12:    $in \leftarrow false, on \leftarrow false, o.refine \leftarrow false$ 
13:   for each query point  $qpoint$  in  $Q_p^*$  originating from  $o$  do
14:     if  $qpoint.wasFound = 1$  then
15:        $in \leftarrow true$  /* octant intersects producer mesh */
16:     else if  $qpoint.wasFound = 2$  then
17:        $on \leftarrow true$  /* octant intersects producer boundary */
18:   if ( $in$  and  $o.isBoundary$ ) or  $on$  then
19:      $o.refine \leftarrow true$ 

```

We test our approach, by adaptively refining the consumer brick and producer arc from level 2 to a maximum level $m = 12$ on the boundary of the intersection area. To test our approach, we start with a consumer brick and a producer arc both refined uniformly to level 2 and use the procedure described above to identify and refine all octants below level 12 on the boundary of the intersection area by one level. We repeat this process iteratively, until no octants are refined anymore.

The refinement procedure gives a good approximation of the intersection area, as can be seen in Figure 16. For further verification we alter the maximum refinement level m and compare the results. The boundary of the intersection area has a fractal dimension of 2. Thus, we would expect the number of maximum level octants to quadruple, when incrementing the maximum level by one. The actual increase in maximum level octants observed during the test runs can be seen in Table 2. The observed ratios match the expectations well. With increasing maximum level, the surface of

m	5	6	7	8	9
# { cons. octants of level m }	28,888	124,496	515,832	2,099,096	8,507,520
ratio m to $m - 1$	–	4.31	4.14	4.07	4.05
# { prod. octants of level m }	36,696	157,496	646,336	2,589,006	10,407,664
ratio m to $m - 1$	–	4.29	4.10	4.01	4.02

Table 2. Number of consumer and producer octants of maximum level m for adaptive refinement around the intersection area in the arc example. The results are displayed for m ranging from 5 to 9. The increase of maximum level octants between the run of level m and the run of level $m - 1$ is shown as well.

the intersection area can be represented with higher accuracy in both meshes, resulting in a ratio even closer to 4.

4.5 Geophysics Simulations

Next to the artificial examples discussed in the previous sections, the Overset algorithm has already been used for real-world applications like mesh coupling in acoustic gravity waves (AGWs) simulations [Snively et al. 2024a, 2025a, 2024b, 2025b, 2023; Zettergren et al. 2025]. The resulting simulation model was scaled to 16,384 cores.

The behavior of the AGWs near their origin on earth’s surface can be simulated by the Model for Acoustic-Gravity wave Interactions and Coupling (MAGIC) [Snively 2013]. The behavior in the ionosphere, where AGWs are ultimately observed, can subsequently be modeled using the Geospace Environment Model for Ion-Neutral Interactions (GEMINI) [Zettergren and Snively 2015]. Both models rely on meshes from the ForestClaw [Calhoun and Burstedde 2017] library, which itself inherits its adaptive mesh refinement capabilities from p4est. In practice, the MAGIC and GEMINI meshes were be coupled efficiently using an implementation of this algorithm in ForestClaw. GEMINI assumes the role of consumer and creates a set of query points for each cell in its curved domain. The queries are supplied with interpolation data by MAGIC, which is the producer in this scenario.

5 Conclusion

In this work, we introduce a new algorithm for the mesh overset of a parallel distributed forest of octrees with another mesh of unrelated partition. The second mesh is defined only by parallel distributed sets of query points. Thus, it may be of almost arbitrary structure. The forest of octrees consists of one or multiple trees, each supplied with its own smooth mapping. Thereby, it can represent a broad range of geometric domains.

We leverage a communication-free, exact partition search of the forest of octrees to match every query point with the process containing it. Based on the results of this search, the query points are sent to and returned from the respective processes. On the leaf level the query points are supplied with the queried data. While the algorithm was developed for a one-directional exchange, a two-directional overset between two forest-of-octree meshes can also be realized by applying the presented method once in each direction, with synergies in message aggregation.

One key aspect of our design is its modularity; since the query points are treated as opaque structures that are passed to problem-dependent callback functions for intersection tests and evaluation. Thus, a query ‘point’ may also be a query ‘cell’ or query ‘object’. This abstraction allows us to extend the proposed algorithm to a variety of overset-related problems covered in this paper,

i.e. adaptive refinement around the intersection area and load balancing via weighted repartitioning, and hints at applications in computational geometry.

We find that the algorithm is quick and scales well to 12,288 cores on the Marvin MPP cluster, in particular when combined with the SFC-based repartitioning of the cells for load balancing. This makes it an excellent candidate for addressing more involved, multi-mesh overset setups. For example, instead of using a forest of octrees as one of the participating meshes, it might be used as a distributed-memory background structure to organize the overset of multiple (unstructured) meshes.

Acknowledgments

We would like to thank Donna Calhoun and Scott Aiton for their support in incorporating this mesh overset algorithm into the ForestClaw software library, and Jonathan Snively as well as Matthew Zettergren for applying and thereby testing the resulting code in a real-world geophysics simulation based on the MAGIC and GEMINI codes. We gratefully appreciate their continuous and insightful feedback on our algorithm and its interface. Furthermore, we would like to thank the support team of the Marvin cluster, above all Dirk Barbi, Jan Steiner and Florian Boecker, for the optimization of the Marvin runtime environment, which made the scaling tests possible.

References

- Carsten Burstedde. 2010. *p4est*: Parallel AMR on Forests of Octrees. <https://www.p4est.org/> (last accessed December 28th, 2025).
- Carsten Burstedde. 2020. Parallel tree algorithms for AMR and non-standard data access. *ACM Trans. Math. Software* 46, 32 (November 2020), 1–31. Issue 4. <https://doi.org/10.1145/3401990>
- Carsten Burstedde, Georg Stadler, Laura Alisic, Lucas C. Wilcox, Eh Tan, Michael Gurnis, and Omar Ghattas. 2013. Large-scale adaptive mantle convection simulation. *Geophysical Journal International* 192, 3 (2013), 889–906. <https://doi.org/10.1093/gji/ggs070>
- Carsten Burstedde, Lucas C. Wilcox, and Omar Ghattas. 2011. *p4est*: Scalable Algorithms for Parallel Adaptive Mesh Refinement on Forests of Octrees. *SIAM Journal on Scientific Computing* 33, 3 (2011), 1103–1133. <https://doi.org/10.1137/100791634>
- Carsten Burstedde, Lucas C. Wilcox, and Tobin Issac. 2010. The "p4est" forest-of-octrees library. <https://github.com/cburstedde/p4est> (last accessed October 24th, 2025).
- Donna Calhoun and Carsten Burstedde. 2017. ForestClaw: A parallel finite volume solver for adaptively refined Cartesian multiblock domains. (2017). arXiv:1703.0317 [cs.MS] Manuscript.
- Fabio Cramer. 2023. *Scientific colour maps*. Fabio Cramer. <https://doi.org/10.5281/zenodo.8409685>
- Michaël Gagnon. 2022. *Development of a Parallel 3D Solid-Solid Overset RANS Method*. Master's thesis. Polytechnique Montréal. <https://publications.polymtl.ca/10351/>
- Mohammadali Hedayat, Amir M. Akbarzadeh, and Iman Borazjani. 2022. A Parallel Dynamic Overset Grid Framework for Immersed Boundary Methods. *Computers & Fluids* 239 (2022), 105378. <https://doi.org/10.1016/j.compfluid.2022.105378>
- William D. Henshaw and Donald W. Schwendeman. 2008. Parallel Computation of Three-Dimensional Flows Using Overlapping Grids With Adaptive Mesh Refinement. *J. Comput. Phys.* 227, 16 (2008), 7469–7502. <https://doi.org/10.1016/j.jcp.2008.04.033>
- Wyatt J. Horne and Krishnan Mahesh. 2019. A Massively-Parallel, Unstructured Overset Method for Mesh Connectivity. *J. Comput. Phys.* 376 (2019), 585–596. <https://doi.org/10.1016/j.jcp.2018.09.053>
- Tobin Isaac, Carsten Burstedde, and Omar Ghattas. 2012. Low-Cost Parallel Algorithms for 2:1 Octree Balance. In *Proceedings of the 26th IEEE International Parallel & Distributed Processing Symposium*, Vol. 1. IEEE, 1730 Massachusetts Avenue, NW Washington, DC, United States, 426–437. <https://doi.org/10.1109/IPDPS.2012.47>
- Tobin Isaac, Carsten Burstedde, Lucas C. Wilcox, and Omar Ghattas. 2015. Recursive algorithms for distributed forests of octrees. *SIAM Journal on Scientific Computing* 37, 5 (2015), C497–C531. <https://doi.org/10.1137/140970963> arXiv:1406.0089 [cs.DC]
- Mikolay Jarkowski, Mark A. Woodgate, George N. Barakos, and Jacek Rokicki. 2014. Towards Consistent Hybrid Overset Mesh Methods for Rotorcraft CFD. *International Journal for Numerical Methods in Fluids* 74, 8 (2014), 543–576. <https://doi.org/10.1002/fld.3861> arXiv:https://onlinelibrary.wiley.com/doi/pdf/10.1002/fld.3861

- Dylan Jude, Jay Sitaraman, and Andrew M. Wissink. 2021. An Octree-Based, Cartesian CFD Solver for Helios on CPU and GPU Architectures.. In *AIAA Scitech 2021 Forum*. AIAA, Reston, Virginia, 0841. <https://doi.org/10.2514/6.2021-0841> arXiv:<https://arc.aiaa.org/doi/pdf/10.2514/6.2021-0841>
- Andrew C. Kirby, Michael J. Brazell, Zhi Yang, Rajib Roy, Behzad R. Ahrabi, Michael K. Stoellinger, Jay Sitaraman, and Dimitri J. Mavriplis. 2019. Wind Farm Simulations using an Overset *hp*-adaptive Approach with blade-resolved Turbine Models. *The International Journal of High Performance Computing Applications* 33, 5 (2019), 897–923. <https://doi.org/10.1177/1094342019832960>
- Robert L. Meakin. 1991. A New Method for Establishing Intergrid Communication Among Systems of Overset Grids. In *10th Computational Fluid Dynamics Conference*. author, Honolulu, 1586. <https://doi.org/10.2514/6.1991-1586> arXiv:<https://arc.aiaa.org/doi/pdf/10.2514/6.1991-1586>
- Guy M. Morton. 1966. *A computer Oriented Geodetic Data Base; and a New Technique in File Sequencing*. Technical Report. IBM Ltd.
- Ralph Noack, David Boger, Robert Kunz, and Pablo Carrica. 2009. Suggar++: An Improved General Overset Grid Assembly Capability. In *19th AIAA Computational Fluid Dynamics*. AIAA, San Antonio, Texas, 3992. <https://doi.org/10.2514/6.2009-3992>
- RW Noack and T Kadanthot. 2002. An octree based overset grid hole cutting method. In *Proceedings of 8th International Conference On Numerical Grid Generation in Computational Field Simulations, Honolulu, HI*. NSF Engineering Research Center of Computational Field Simulation, Mississippi, USA, 783–792.
- Stéphanie Péron and Christophe Benoit. 2013. Automatic Off-Body Overset Adaptive Cartesian Mesh Method Based on an Octree Approach. *J. Comput. Phys.* 232, 1 (2013), 153–173. <https://doi.org/10.1016/j.jcp.2012.07.029>
- Beatrice Roget and Jayanarayanan Sitaraman. 2014. Robust and efficient overset grid assembly for partitioned unstructured meshes. *J. Comput. Phys.* 260 (2014), 1–24. <https://doi.org/10.1016/j.jcp.2013.12.021>
- Jorg Schluter, Xiaohua Wu, Edwin van der Weide, Seonghyeon Hahn, Juan Alonso, and Heinz Pitsch. 2005. Multi-Code Simulations: A Generalized Coupling Approach. In *17th AIAA Computational Fluid Dynamics Conference*. AIAA, Toronto, Ontario, Canada, 4997. <https://doi.org/10.2514/6.2005-4997> arXiv:<https://arc.aiaa.org/doi/pdf/10.2514/6.2005-4997>
- Thorsten Schwarz. 2005. *Ein blockstrukturiertes Verfahren zur Simulation der Umströmung komplexer Konfigurationen*. Technical Report. TU Braunschweig. <https://elib.dlr.de/44080/>
- Orxan Shibliyev and Ibrahim Sezai. 2021. Overset Grid Assembler and Flow Solver with Adaptive Spatial Load Balancing. *Applied Sciences* 11 (2021), no. 5132. <https://doi.org/10.3390/app11115132>
- Jonathan B. Snively. 2013. Mesospheric Hydroxyl Airglow Signatures of Acoustic and Gravity Waves Generated by Transient Tropospheric Forcing. *Geophysical Research Letters* 40, 17 (2013), 4533–4537. <https://doi.org/10.1002/grl.50886> arXiv:<https://agupubs.onlinelibrary.wiley.com/doi/pdf/10.1002/grl.50886>
- Jonathan B Snively, Donna Calhoun, Scott Aiton, Carsten Burstedde, Hannes Brandt, Tim Griesbach, Benedict Pineyro, Pavel Inchin, Roberto Sabatini, Michael Hirsch, and Matthew D Zettergren. 2024a. Scalable Modeling of Infrasound Propagation from Transient Sources in Surface-to-Exobase Domains. AGU24 Annual Meeting.
- Jonathan B Snively, Donna Calhoun, Scott Aiton, Carsten Burstedde, Hannes Brandt, Tim Griesbach, Benedict Pineyro, Pavel Inchin, Roberto Sabatini, Michael Hirsch, and Matthew D Zettergren. 2025a. Scalable Modeling of Infrasound Propagation in Realistic Environments from Surface to Exobase. AGU25 Annual Meeting.
- Jonathan B Snively, Donna Calhoun, Scott Aiton, Carsten Burstedde, Hannes Brandt, Tim Griesbach, Benedict Pineyro, Sehin Mesfin, Jaime Aguilar Guerrero, Christopher James Heale, Pavel Inchin, Roberto Sabatini, Michael Hirsch, and Matthew D Zettergren. 2024b. Scalable Modeling of Acoustic-Gravity Wave-driven Traveling Ionospheric Disturbances. AGU24 Annual Meeting.
- Jonathan B Snively, Donna Calhoun, Scott Aiton, Carsten Burstedde, Hannes Brandt, Tim Griesbach, Benedict Pineyro, Sehin Mesfin, Jaime Aguilar Guerrero, Christopher J Heale, Pavel Inchin, Roberto Sabatini, Michael Hirsch, and Matthew D Zettergren. 2025b. Scalable Modeling of Acoustic-Gravity Wave Propagation and Evolutions from Impulsive Sources. AGU25 Annual Meeting.
- Jonathan B Snively, Donna Calhoun, Scott Aiton, Carsten Burstedde, Hannes Brandt, Michael Hirsch, Jaime Aguilar Guerrero, Christopher James Heale, Pavel Inchin, Sehin Mesfin, Benedict Pinyero, Roberto Sabatini, and Matthew D Zettergren. 2023. Scalable Modeling of Acoustic-Gravity Wave Processes in the Ionosphere, Thermosphere, and Mesosphere (ITM). AGU23 Fall Meeting.
- Joseph L. Steger, F. Carroll Dougherty, and John A. Benek. 1983. A Chimera grid scheme. *K.N. Ghia, U. Chia (Eds.), Advance in Grid Generation, ASME FED* 5 (1983), 59 – 69.
- Norman Suhs, Stuart Rogers, and William Dietz. 2002. PEGASUS 5: An Automated Pre-Processor for Overset-Grid CFD. In *32nd AIAA Fluid Dynamics Conference and Exhibit*. AIAA, St. Louis, Missouri, 3186. <https://doi.org/10.2514/6.2002-3186> arXiv:<https://arc.aiaa.org/doi/pdf/10.2514/6.2002-3186>
- Hari Sundar, Rahul Sampath, and George Biros. 2008. Bottom-up construction and 2:1 balance refinement of linear octrees in parallel. *SIAM Journal on Scientific Computing* 30, 5 (2008), 2675–2708. <https://doi.org/10.1137/070681727>

- Matthew D Zettergren, Donna Calhoun, Jonathan B Snively, Carsten Burstedde, Hannes Brandt, Pavel Inchin, Michael Hirsch, Tim Griesbach, Scott Aiton, and Kshitija Deshpande. 2025. Numerical Modeling of Ionospheric Responses to Ground-level, Anthropogenic Sources. AGU25 Annual Meeting.
- Matthew D. Zettergren and Jonathan B. Snively. 2015. Ionospheric response to infrasonic-acoustic waves generated by natural hazard events. *Journal of Geophysical Research: Space Physics* 120, 9 (2015), 8002–8024. <https://doi.org/10.1002/2015JA021116> arXiv:<https://agupubs.onlinelibrary.wiley.com/doi/pdf/10.1002/2015JA021116>
- Matthew D. Zettergren and Jonathan B. Snively. 2019. Latitude and Longitude Dependence of Ionospheric TEC and Magnetic Perturbations From Infrasonic Acoustic Waves Generated by Strong Seismic Events. *Geophysical Research Letters* 46, 3 (2019), 1132–1140. <https://doi.org/10.1029/2018GL081569>
- Ran Zhao, Chao Li, Xiaowei Guo, Sen Zhang, Xi Yang, Tao Tang, and Canqun Yang. 2024. *A Motion Trace Decomposition-based overset grid method for parallel CFD simulations with moving boundaries*. Association for Computing Machinery, New York, NY, USA, 411–420. <https://doi.org/10.1145/3673038.3673102>

A Application to Disjoint Communicators

In Section 4 we only performed tests for congruent consumer and producer communicators with both of them being equal to the global communicator. However, the overset algorithm can also be performed for disjoint or partially overlapping communicators. How the code is distributed between the communicators is shown in the pseudocode of Algorithm 3.

We adapt our implementation to deal with disjoint or partially overlapping communicators. To achieve this, without loss of generality we define the consumer communicator as the subset $[0, Q)$ and the producer communicator as the subset $[P, P_{\text{global}})$ of MPI_COMM_WORLD , where P_{global} denotes the global process count.

The overset algorithm requires extensive point-to-point communication between processes from the two communicators. Since both communicators are contiguous subsets of MPI_COMM_WORLD , it suffices to exchange their respective global communicator offsets 0 and P . Based on this information, the point-to-point communication between consumer and producer can be performed on the global communicator.

One of the major differences between the congruent and the disjoint case is the communication of basic producer mesh information such as the global first positions F , the amount of producer trees and the size of the producer communicator. If the communicators are congruent, or the producer communicator completely contains the consumer communicator, the consumer processes can access this information directly. In all other cases, the producer root sends the information to the consumer root for broadcasting on the consumer communicator. The length of F depends on the amount of producer processes, so these pieces of data need to be communicated in separate iterations.

We tested our implementation for the arc example as described in Section 4.2.1 for $Q = P = \frac{P_{\text{global}}}{2}$. The results are too similar to the strong scaling results for congruent communicators (see Figure 12) to justify the inclusion of another plot. In particular, the run time does not improve when switching from $P = Q$ processes in congruent communicators to the same amount of producer and consumer processes in disjoint communicators. This is to be expected, since there is little potential for overlap between the consumer and producer tasks. The producer processes have to wait for the consumer processes to finish their partition search and send the resulting query point buffers, before they can start the local search and evaluation. Vice versa, the consumer processes have to wait until the producer processes return the evaluation data to incorporate it into their local mesh.

So, the disjoint communicator approach does not yield any advantages for the mesh overset itself. However, it offers the possibility to overlap the mesh overset with other producer or consumer specific tasks, which can be performed while waiting for the partition/local search results. In particular, it is possible to switch to disjoint communicators without losing scalability.

B Reproducing Examples

The numerical applications presented in Section 4 cover different example settings implemented in the `example/multi` directory of the `p4est` library [Burstedde et al. 2010] under commit id `b34b7162`.

The examples can be executed by calling

```
mpirun -np ${n} ./example/multi/p{4,8}est_overlap
```

with the following command line parameters

- e Specify the mappings for the examples.
 - 0 - Arc and brick mapping from Section 4.2.1 with switched consumer and producer roles.
 - 1 - Arc and brick mapping from Section 4.2.1.
 - 2 - Rotated unit square mappings from Section 4.1.
 - 3 - Un-rotated unit square mappings from Section 4.1.
- r Specify the refinement method.
 - 0 - Refinement around the intersection area from Section 4.4.
 - 1 - Refinement around a specific point from Section 4.2.1.
 - 2 - Artificial refinement based on child-id and rank of the octants.
 - 3 - Refinement around a pentagon from 4.1.2.
- l Specify if the load balancing from Section 4.3 should be enabled. Defaults to false.
- a, -b Specify the consumer and producer communicator sizes. The consumer communicator covers the range $[0, a)$ of ranks. The producer communicator covers the range $[b, n)$. Both default to the range $[0, n)$.
- c, -p Specify the initial uniform refinement level of consumer and producer mesh. Both default to 0.
- m Specify the maximum refinement level for the iterative refinement. Defaults to 0.
- v, -t Specify the form of the output. If `v` is true, `vtk` output is generated for both meshes. If `t` is true, a list of all query points with their evaluation data is printed to the console. Both default to false.

The scaling tests for the unit square example with adaptive refinement from 4.1 were performed calling

```
./example/multi/p4est_overlap -c 2 -p 2 -r 3 -m 20 -e {2,3}
```

with `e` being switched for rotated and unrotated versions. The scaling tests for the arc example from Section 4.2.2 and Section 4.3 were performed calling

```
./example/multi/p8est_overlap -c {5,6} -p {4,5} -r 1 -m {9,10} -e 1 -l {0,1}
```

with `c`, `p` and `m` being switched for the small and middle example and `l` being switched for enabling or disabling load balancing. Similarly, the weak scaling tests were performed calling:

```
./example/multi/p8est_overlap -c {4,5,6,7} -p {3,4,5,6} -r 1 -m {8,9,10,11}
-e 1 -l 1
```

Finally, the scaling tests for disjoint communicators from Appendix A were performed calling:

```
./example/multi/p8est_overlap -c {5,6} -p {4,5} -r 1 -m {9,10} -e 1
-a n/2 -b n/2
```